

Aberration-Corrected Z-Contrast Scanning Transmission Electron Microscopy of CdSe Nanocrystals

James R. McBride,[†] Tadd C. Kippeny,[†] Stephen J. Pennycook,[†] and Sandra J. Rosenthal^{*,†}

Oak Ridge National Laboratory, Condensed Matter Sciences Division, Oak Ridge, Tennessee 37831, and Vanderbilt University, Department of Chemistry, Nashville, Tennessee 37235

Received April 22, 2004; Revised Manuscript Received May 17, 2004

ABSTRACT

Aberration-corrected atomic number contrast scanning transmission electron microscopy (Z-STEM) was used to study CdSe nanocrystals prepared using different surfactants. With an optimal probe size of 0.8 Å, unprecedentedly detailed images of the nanocrystal's lattice structure and surface morphology were obtained. This level of detail is important for the characterization of nanomaterials because of the high sensitivity of the nanocrystal's properties to minute changes in structure. As an example of the power of this technique, a sample of CdSe nanocrystals prepared using trioctylphosphine oxide (TOPO) as the surfactant was compared to a sample of CdSe prepared using a mixture of TOPO and hexadecylamine (HDA). Z-STEM reveals striking differences in nanocrystal morphology as the result of the addition of HDA.

Semiconductor nanocrystals are of primary interest to several fields of research because of their unique properties. They exhibit quantum confinement effects such as size-dependent absorption and emission, which allows for size-tunable optical and electronic properties for applications in photovoltaics,^{1–3} photocatalysis,^{4–7} bioassays,^{3,8–12} and electronics.^{13–16} These unique properties are sensitive to minuscule changes in size and shape requiring a characterization technique with a subnanometer level of sensitivity and precision. Furthermore, information regarding surface structure would be an enormous asset for the development of nanocrystal-based devices and applications. For example, core/shell nanocrystals systems rely on a surface-passivating layer to obtain high fluorescent yields. Surface coverage on the order of a monolayer can significantly impact the fluorescent quantum yield.^{17–21} Bulk characterization techniques such as XRD and absorption and fluorescence measurements give details only about the ensemble of nanocrystals, forming an average, yet incomplete, picture of the nanocrystal sample.

Electron microscopy techniques such as high-resolution transmission electron microscopy (HRTEM) have been the primary technique used to characterize nanocrystal size and shape. HRTEM allows us to analyze individual nanocrystals and obtain an average size distribution.^{22,23} Unfortunately,

it can be very difficult to determine the precise shape and size of the nanocrystal because of nanocrystal movement under the electron beam and poor contrast near the surface of the nanocrystal. Additionally, phase-contrast imaging relies on lattice fringes, which arise from the periodic structure of the crystal lattice. This periodicity is broken at the surface and nearby lattice defects, complicating image interpretation.

Z-contrast scanning transmission electron microscopy (Z-STEM), however, can provide highly detailed images of the nanocrystal surface, 3D information, and mass contrast simultaneously, which can all be directly discerned from the image. Z-STEM uses an incoherent imaging process, which yields images that are directly interpretable to the structure of the object being observed. With this technique, combined with a spherical aberration (C_s)-corrected STEM, highly spatially resolved images can be obtained that are able to show subtle details about the shape and faceting of nanocrystals with near sub-angstrom precision.

In this letter, we used aberration-corrected Z-STEM to image CdSe nanocrystals prepared by two different surfactant mixtures. Striking differences in morphology are observed with an overall improvement in shape when hexadecylamine (HDA) is used.

The two CdSe samples used for comparison were synthesized using similar techniques to that of Peng et al.²⁴ and that of Talapin et al., who includes HDA into the reaction mixture.²⁵ For the trioctylphosphine oxide (TOPO)-only sample, the reaction solution consisted of a 2.5:1.84 by mass

* Corresponding author. E-mail: sandra.j.rosenthal@vanderbilt.edu.

[†] Oak Ridge National Laboratory.

[‡] Vanderbilt University.

solution of dimethyl cadmium (Strem, vacuum distilled), selenium metal (shot, Strem, as received), and tributylphosphine (Strem, as received). A volume of 6 mL of the reaction solution was injected into 12 g of trioctylphosphine oxide (90%, Aldrich) maintained at 360 °C. As soon as the solution temperature dropped to 300 °C, an additional amount (0.5–4 mL, depending on the final size desired) of the concentrated reaction solution (2.5:1:21 by mass) was added. The nanocrystals were then allowed to grow at 300 °C. The hexadecylamine (HDA) sample was prepared in a similar fashion with a few modifications. Briefly, 375 μL of dimethyl cadmium and 0.288 g of selenium powder in 30 mL of tributyl phosphine constitute the reaction solution. The reaction solution is injected into a mixture of 43.2 g of TOPO, 17.85 g of HDA, and 0.855 g dodecyl phosphonic acid (DPA), which is an analogue of a key impurity found in technical-grade TOPO, at 300 °C for crystal nucleation.^{26–28} The temperature is then lowered to 265–270 °C for crystal growth. Growth was monitored for both samples by taking absorption spectra of aliquots removed from the flask until the exciton peak ceased to narrow, at which point the reaction was stopped by removing the heat source.

Samples were washed three times by precipitation in methanol followed by centrifugation. It is important to remove any excess starting material to minimize contamination under the electron beam. After washing, the samples were dissolved in toluene, dropped onto an ultrathin carbon-coated TEM grid (Ted Pella Inc.), and allowed to dry.

Atomic-resolution Z-contrast imaging was performed using a VG microscopes model HB603U STEM operating at 300 kV fitted with a C_s corrector from Nion. The optimal probe size has been measured to be 0.78 Å with a theoretical limit of 0.5 Å.²⁹ The operation and data collection were done by Digital Micrograph running on a Pentium 4 1.7-GHz personal computer.

Z-contrast STEM achieves several advantages over conventional TEM methods by using incoherently scattered electrons that are collected by a high-angle annular dark field (HAADF) detector to form an image. Incoherent images are more intuitive than traditional coherent images and can be directly related to the structure of the object being imaged.^{30,31} Additionally, the intensity of the scattered electrons is dependent on the mass of the incident atom, yielding spatially resolved chemical information. The incoherent scattering of the electron is described by the Rutherford scattering equation where

$$\frac{d\sigma(\theta)}{d\Omega} = \frac{e^4 Z^2}{16(E_0)^2 \sin^4 \frac{\theta}{2}}$$

The left side of the equation denotes different scattering cross sections as a function of the scattering angle θ . E_0 is the incident beam energy, and e is the electron charge, with Z being the atomic number of the scattering nucleus.³² This equation predicts that the intensity of the scattered electrons will be dependent on the square of the atomic number (Z^2) for a sufficiently high angular range. For this reason, mass

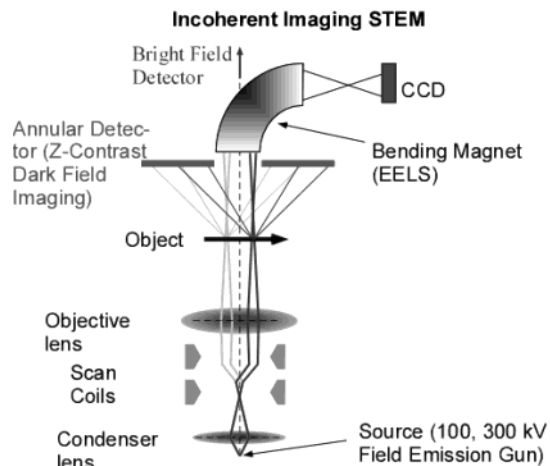


Figure 1. Incoherent imaging STEM. A highly focused electron beam (minimum diameter of 0.8 Å fwhm) is scanned across the sample to form an image. The HAADF detector collects the electrons that are scattered at high angles, while the ones scattered at small angles continue through to form a bright-field image or to conduct EELS analysis.

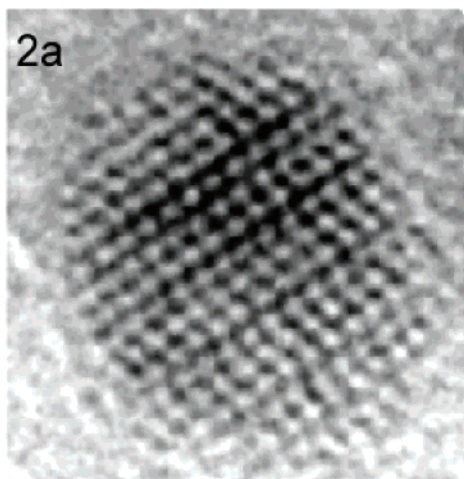
contrast can be observed directly from the image. A typical setup for Z-STEM is shown in Figure 1.

Intensity is also dependent on sample thickness, allowing for the direct measurement of an object's 3D structure from the image. For example, in a crystalline specimen in channeling orientation, high-angle scattering is predominantly from the 1s Bloch states of the fast electrons in the crystal. These states have negligible overlap, so the intensities for each column are independent of each other. The cross talk that does occur is due to aberrations from the electron probe interacting with adjacent columns.³³ A comparison between two comparably orientated CdSe nanocrystals imaged under HRTEM and Z-STEM is shown in Figure 2. False color has been added to the Z-STEM image to emphasize the importance of the image intensity. Unlike the conventional HRTEM image, chemical and structural information can be learned directly from the intensity in the raw Z-STEM image. For example, the Cd and Se columns can be assigned from the intensity difference found in the raw image, as indicated by the line profile in Figure 2c. With this information, the Cd-rich (001) and the Se-rich (001') surfaces can then be assigned by following the alternating intensities to the surface. Additionally, because the electrons that are detected are incoherently scattered, phase contrast that arises from interactions between the electron beam and a crystal lattice is not needed to form an image. As a result, amorphous regions and single atoms can be imaged. The amorphous oxide layer, which has been enclosed by a white circle, can be clearly seen in the Z-STEM image in Figure 2c. The spots seen in this are the remains of the outer surface of the nanocrystal that has been oxidized. Individual atoms and atomic clusters can readily be found in this region.

The advent of the spherical aberration (C_s) corrector has greatly reduced the overall beam profile by correcting up to third-order aberrations successfully. The corrector uses a software-driven set of quadrupoles and octupoles, which work to correct for aberrations inherent in conventional round

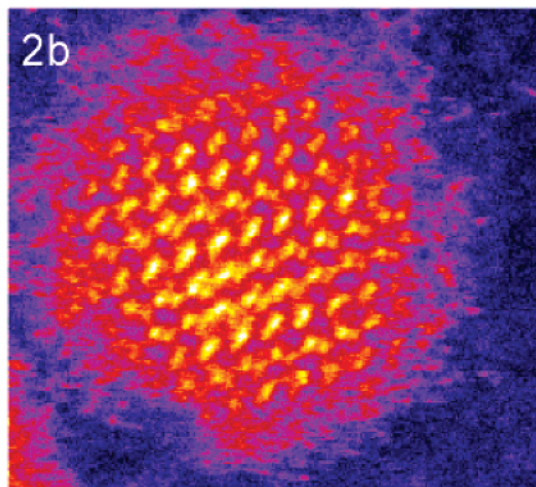
Advantages of Z-STEM

Philips CM20 200 kV TEM



3 nm

VG HB 603U 300 kV STEM



3 nm

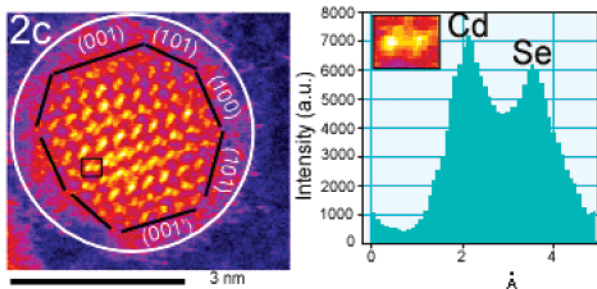
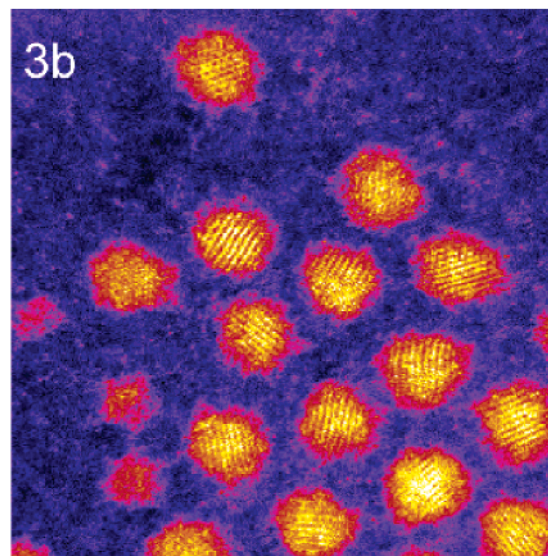
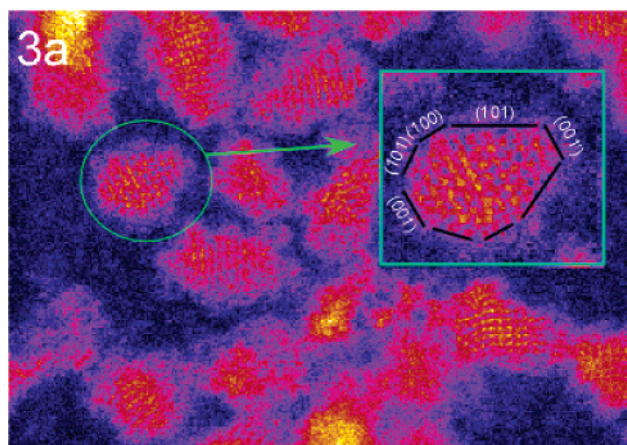


Figure 2. Advantages of Z-STEM. Differences between TEM (2a) and Z-STEM (2b) imaging for a CdSe nanocrystal can be seen by comparing these two similarly orientated nanocrystals. The major advantage of Z-STEM is that the image intensity is dependent on the chemical composition of the object being imaged. The line profile across a CdSe “dumbbell” (2c) illustrates how chemical information can be learned directly from the image. In the bottom image (2c), a white circle was used to highlight the amorphous oxide region containing single atoms and atomic clusters, and the surface of the nanocrystal has been outlined in black. Also, the various facets have been labeled, with (001) indicating the Se face.

Z-STEM Images of CdSe



6 nm

Figure 3. Z-STEM Images of CdSe. Images of a sample of TOPO-prepared CdSe (3a) and an image of TOPO/HDA-prepared CdSe (3b) are shown. The addition of HDA appears to make nanocrystals with more uniform shapes and sizes. The shape differences seen in 3a would be very difficult to see using TEM. The Z-STEM images have been artificially colored.

lenses. At 300 kV, a 0.5-Å probe could theoretically be achieved using the C_s -corrected STEM.³⁴ The advantages of the smaller probe size are a higher signal-to-noise ratio and the ability to image smaller lattice spacing. This advantage becomes clear when this technique is applied to the imaging of nanocrystals because tilting the specimen is not practical due to the constant movement of the nanocrystals under the electron beam.

A comparison between the TOPO- and the HDA/TOPO-prepared samples is shown in Figure 3. In both images, the benefit of the C_s corrector and the small probe size is manifested by the large number of lattice-resolved nanocrystals. Because the nanocrystals are free to rotate, obtaining a good lattice-resolved image is dependent on the orientation of the nanocrystal during image capture. As the probe size decreases, the number of lattice-resolved nanocrystals increases because of the improved ability to image nanocrystals

off axis. The small features near the surface that are seen would be very difficult to detect using traditional HRTEM because there is very little material to form a phase-contrast image.

Interestingly, a striking difference between the two images can be seen. Although the size of the nanocrystals differs only by 0.3 nm on average, their overall shape is markedly different. The TOPO-prepared CdSe nanocrystals appear to be elongated with some exhibiting an ovoid shape. For example, the nanocrystal circled in Figure 3a shows a definite narrowing along the *C* axis, which is parallel to the surface plane. The inhomogeneous faceting of this sample is likely the result of preferential growth along this axis. From this image, the orientation of the Cd and Se dumbbells can be determined, allowing us to assign the narrow end of the nanocrystal as being capped by the Se-rich (001') face. This directly assigns the Se-rich face as the primary growth face. Additionally, it has been reported previously that CdSe nanocrystals prepared by the TOPO-only method are cadmium rich.³⁵ It is believed that the excess Cd found in the TOPO-only nanocrystals resides in these elongated (101) facets where there are two Se dangling bonds at each Se surface site. The images indicate that the (101) is dominant over the (100) faces, which is likely the reason for the nonstoichiometry.

In contrast, the nanocrystals prepared by the TOPO/HDA method shown in Figure 3b are extremely uniform in size and shape. The nanocrystals seem to be truncated evenly on either side, suggesting a lack of preferential growth or more controlled growth as seen in the TOPO sample. Because a majority of the nanocrystals are of the same size and shape, spontaneous 2D arrays form exhibiting the same hexagonal structure as the nanocrystals.

Parts a and b of Figure 4 show high-resolution images of CdSe nanocrystals from the TOPO/HDA sample with the [100] and [001] axis orientations, respectively. In the [100] orientation, only a few Cd and Se columns are resolved in the raw image, likely because of the crystal being tilted slightly off axis. Although there is an oxide layer coating the surface, it is sufficiently thin in some areas to allow for the exact surface of the nanocrystal to be seen. Unlike the TOPO-only nanocrystals, (100) faces now dominate the sides of the nanocrystal. The [001]-orientated nanocrystal, Figure 4b, has all of the atomic columns resolved, and the hexagonal, wurtzite lattice structure is clearly visible. In this orientation, no mass contrast is expected because the Cd and Se columns are aligned on top of each other. Additionally, the change in intensity across the (001) face of the nanocrystal suggests nanocrystal faceting.³⁶ The uniform shape that is found in the TOPO/HDA sample might be the result of the slower growth rate observed with the addition of HDA to the reaction mixture.²⁰ This slower growth mechanism allows for surface reconstruction, which is necessary for achieving high fluorescence quantum yields.²⁵ Also, it has been shown that the impurity analogue, in our case, DPA, enhances the growth along the *C* axis, which is an unwanted effect.³⁷ The addition of HDA seems to prevent this unidirectional growth. The structural differences seen in the

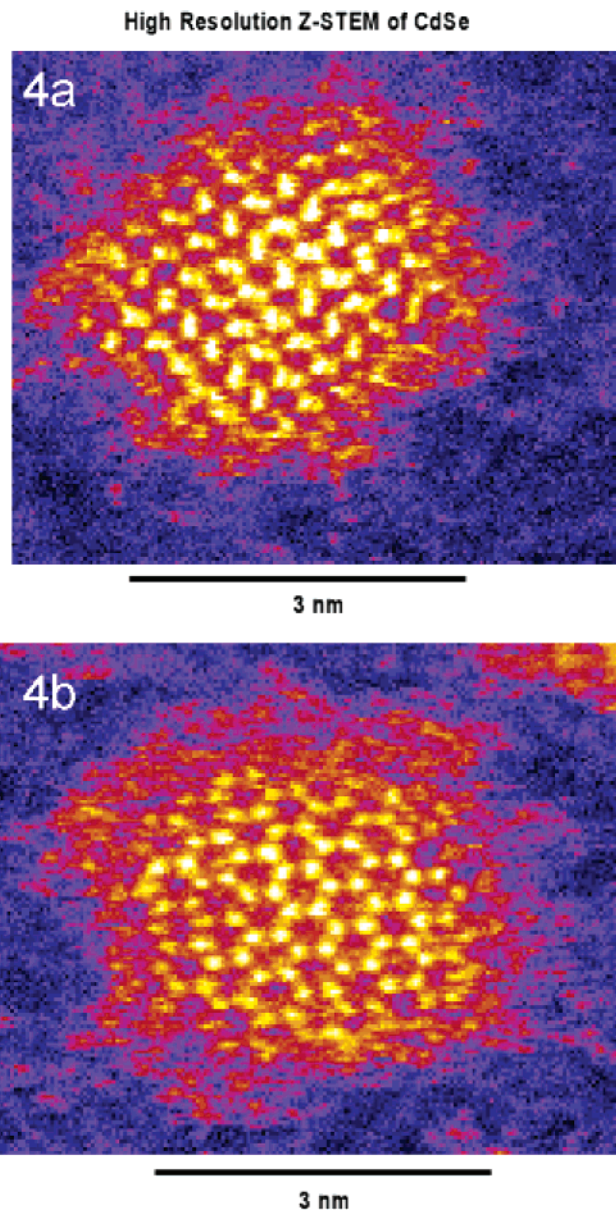


Figure 4. High-resolution Z-STEM images of CdSe. High-resolution Z-STEM images of a TOPO/HDA-prepared CdSe nanocrystal in the [100] (4a) and [001] (4b) orientations, respectively. In both images, a surface oxide can be seen along with several single atoms. The Z-STEM images have been artificially colored to emphasize mass contrast.

images seem to support these two conclusions. The elimination of the elongated, (101), facets is also accompanied by the elimination of the excess Cd reported previously. Recent Rutherford backscattering spectroscopy analysis that we have performed indicates that the Cd-to-Se ratio for the TOPO/HDA-prepared sample is near unity, supporting the claim that excess Cd is located on the facets.

Z-contrast imaging shows great promise for characterizing nanocrystals and other nanomaterials. The extremely high resolution, detail, and chemical information obtained from this technique cannot be achieved using conventional TEM techniques. Subtle changes on the surface or in the overall shape can be seen that should allow for a better understanding of the growth kinetics, surface reconstruction, and ligand

effects of CdSe and other nanocrystal systems. In this case, the addition of HDA to the reaction mixture not only narrowed the size distribution as reported elsewhere but also greatly reduced the number of shape anomalies compared to the number for the traditional TOPO method. Additionally, Z-STEM provides supporting evidence for the location of the excess Cd in TOPO-prepared CdSe nanocrystals.³⁵

Acknowledgment. We would like to thank Andrew Lupini and the Pennycook research group for assistance with the microscope. We also would like to thank Leonard Feldman for the use of the accelerator lab for the RBS studies. Funding for this research was provided by a Vanderbilt Institute of Nanoscience and Engineering fellowship and by the Department of Energy (grant DE-FG0202ER45957).

Supporting Information Available: RBS data used to calculate the ratio of Cd to Se for the HDA CdSe nanocrystals. This material is available free of charge via the Internet at <http://pubs.acs.org>.

References

- (1) Swafford, L. A.; Rosenthal, S. J. Molecular and Nanomaterial-Based Photovoltaics. In *Molecular Nanoelectronics*; Reed, E. M. A., Lee, T., Eds.; American Scientific Publishers: Stevenson Ranch, CA, 2003.
- (2) Greenham, N. C.; Peng, X.; Alivisatos, A. P. *Phys. Rev. B* **1996**, *54*, 17628.
- (3) Erwin, M. M.; Kadavanich, A. V.; McBride, J.; Kippeny, T.; Pennycook, S.; Rosenthal, S. J. *Eur. J. Phys. D* **2001**, *16*, 275–277.
- (4) Henglein, A. *Pure Appl. Chem.* **1984**, *56*, 1215.
- (5) Henglein, A. *Ber. Bunsen-Ges. Phys. Chem. Chem. Phys.* **1997**, *101*, 1562.
- (6) Nanda, J.; Sapra, S.; Sarma, D.; Chandrasekharan, N.; Hodes, G. *Chem. Mater.* **2000**, *12*, 1018.
- (7) Kho, R.; Nguyen, L.; Torres-Martinez, C. L.; Mehra, R. K. *Biophys. Res. Commun.* **2000**, *272*, 29.
- (8) Dubertret, B.; Skourides, P.; Norris, D. J.; Noireaux, V.; Brivanlou, A. H.; Libchaber, A. *Science* **2002**, *298*, 1759.
- (9) Gerion, D.; Parak, W. J.; Williams, S. C.; Zanchet, D.; Micheel, C. M.; Alivisatos, A. P. *J. Am. Chem. Soc.* **2002**, *124*, 7070.
- (10) Tomlinson, I. D.; Mason, J.; Blakely, R. D.; Rosenthal, S. J. *Biotechnol. Protocols*, in press.
- (11) Rosenthal, S. J.; Tomlinson, I. D.; Adkins, E. M.; Schroeter, S.; Adams, S.; Swafford, L.; McBride, J.; Wang, Y.; DeFelice, L. J.; Blakely, R. D. *J. Am. Chem. Soc.* **2002**, *124*, 4586.
- (12) Wu, X.; Liu, H.; Lui, J.; Haley, K. N.; Treadway, J. A.; Larson, P. J.; Ge, N.; Peale, F.; Bruchez, M. P. *Nat. Biotechnol.* **2003**, *21*, 41.
- (13) Klein, D. L.; Roth, R.; Lim, A. K. L.; Alivisatos, A. P.; McEuen, P. L. *Nature* **1997**, *389*, 669.
- (14) Gao, M. Y.; Lesser, C.; Kirstein, S.; Mohwald, H.; Rogach, A. L.; Weller, H. *J. Appl. Phys.* **2000**, *87*, 2297.
- (15) Konenkamp, R.; Hoyer, P.; Wahi, A. *J. Appl. Phys.* **1996**, *79*, 7029.
- (16) Vlasov, Y. A.; Yao, N.; Norris, D. J. *Adv. Mater.* **1999**, *11*, 165.
- (17) Wang, X.; Qu, L.; Zhang, J.; Peng, X.; Xiao, M. *Nano Lett.* **2003**, *3*, 1103.
- (18) Myung, N.; Bae, Y.; Bard, A. J. *Nano Lett.* **2003**, *3*, 747.
- (19) Manna, L.; Scher, E. C.; Li, L.; Alivisatos, A. P. *J. Am. Chem. Soc.* **2002**, *124*, 7136.
- (20) Donega, C. M.; Hickey, S. G.; Wuister, S. F.; Vanmaekelbergh, D.; Meijerink, A. *J. Phys. Chem. B* **2003**, *107*, 489.
- (21) Landes, C.; Burda, C.; Braun, M.; El-Sayed, M. A. *J. Phys. Chem. B* **2001**, *105*, 2981.
- (22) Kadavanich, A. V.; A. M.; Tolbert, S. H.; Peng, X.; Schlamp, M. C.; Lee, J. C.; Alivisatos, A. P. *Adv. Microcryst. Nanocryst. Semicond. 1996, Symp.* 1996.
- (23) Shiang, J. J.; Kadavanich, A. V.; Grubbs, R. K.; Alivisatos, A. P. *J. Phys. Chem.* **1995**, *99*, 17417.
- (24) Peng, X. G.; Wickham, J.; Alivisatos, A. P. *J. Am. Chem. Soc.* **1998**, *120*, 5343.
- (25) Talapin, D. V.; Rogach, A. L.; Kronowski, A.; Haase, M.; Weller, H. *Nano Lett.* **2001**, *1*, 207.
- (26) Peng, Z. A.; Peng, X. *J. Am. Chem. Soc.* **2001**, *123*, 1389.
- (27) Reis, P.; Bleuse, J.; Pron, A. *Nano Lett.* **2002**, *2*, 781.
- (28) Reis, P.; Caryon, S.; Bleuse, J.; Pron, A. *Synth. Met.* **2003**, *139*, 649.
- (29) Nellist, P. D.; Pennycook, S. J. *Phys. Rev. Lett.* **1998**, *81*, 4156.
- (30) Pennycook, S. J.; Nellist, P. D. Z-Contrast Scanning Transmission Electron Microscopy. In *Impact of Electron Scanning Probe Microscopy on Materials Research*. Rickerby, G. V. D., Valdre, U., Ed.; Kluwer Academic Publishers: Norwell, MA, 1999.
- (31) Nellist, P. D.; S. J. P. *Ultramicroscopy* **1999**, 111.
- (32) Williams, D. B.; Carter, C. B. *Transmission Electron Microscopy: A Textbook for Materials Science*. Plenum Press: New York, 1996.
- (33) Pennycook, S. J.; Jesson, D. E. *Phys. Rev. Lett.* **1990**, *64*.
- (34) Krivanek, O. L.; P. D. N.; Dellby, N.; Murfitt, M. F.; Szilagy, Z.; *Ultramicroscopy* **2003**, *96*, 229.
- (35) Taylor, J.; T. K.; Rosenthal, S. J. *J. Clust. Sci.* **2001**, *12*, 571.
- (36) Kadavanich, A. V.; Kippeny, T.; Erwin, M. M.; Pennycook, S. J.; Rosenthal, S. J. *J. Phys. Chem. B* **2001**, *105*, 361.
- (37) Manna, L.; Scher, E. C.; Alivisatos, A. P. *J. Am. Chem. Soc.* **2000**, *122*, 12700.

NL049406Q